A Method for Retrieving Vertical Air Velocities in Convective Clouds over the Tibetan Plateau from TIPEX-III Cloud Radar Doppler Spectra

Jiafeng Zheng [1,2], Liping Liu [2,*], Keyun Zhu [1], Jingya Wu [3] and Binyun Wang [1]

[1]   Plateau Atmosphere and Environment Key Laboratory of Sichuan Province, School of Atmospheric Sciences, Chengdu University of Information Technology, Chengdu 610225, China; zjf1988@cuit.edu.cn (J.Z.); zhuky@cuit.edu.cn (K.Z.); bywang@cuit.edu.cn (B.W.)
[2]   State Key Lab of Severe Weather, Chinese Academy of Meteorological Sciences, Beijing 100081, China
[3]   Institute of Atmospheric Physics, Chinese Academy of Sciences, Beijing 100029, China; wujingya@mail.iap.ac.cn
*   Correspondence: lpliu@camscma.cn; Tel.: +86-010-6840-6768

Abstract: In the summertime, convective cells occur frequently over the Tibetan Plateau (TP) because of the large dynamic and thermal effects of the landmass. Measurements of vertical air velocity in convective cloud are useful for advancing our understanding of the dynamic and microphysical mechanisms of clouds and can be used to improve the parameterization of current numerical models. This paper presents a technique for retrieving high-resolution vertical air velocities in convective clouds over the TP through the use of Doppler spectra from vertically pointing Ka-band cloud radar. The method was based on the development of a "small-particle-traced" idea and its associated data processing, and it used three modes of radar. Spectral broadening corrections, uncertainty estimations, and results merging were used to ensure accurate results. Qualitative analysis of two typical convective cases showed that the retrievals were reliable and agreed with the expected results inferred from other radar measurements. A quantitative retrieval of vertical air motion from a ground-based optical disdrometer was used to compare with the radar-derived result. This comparison illustrated that, while the data trends from the two methods of retrieval were in agreement while identifying the updrafts and downdrafts, the cloud radar had a much higher resolution and was able to reveal the small-scale variations in vertical air motion.

Keywords: vertical air velocity; millimeter-wave cloud radar; convective cloud; Tibetan Plateau

1. Introduction

The Tibetan Plateau (TP) is the largest and highest plateau on our planet, with an average altitude of over 4000 m and a complicated terrain. Because of strong dynamic and thermal effects of its landmass, the TP can significantly impact the circulation, climate, and weather of East Asia and the entire Northern Hemisphere [1–5]. In the summertime, vertical air motion over the TP is stronger than over other areas because of significant ground heating, leading to the frequent occurrence of convective cells. Several early investigations suggested that convective clouds over the TP account for approximately 60% of the total cloud amount, with convective cell occurrence rates 1.5 times higher than over other regions of China. Indeed, there may be up to 300 convective cells on the plateau per day [6,7]. Under favorable synoptic conditions, these convective cells can move eastwards to central and eastern China and cause severe weather [8,9]. Moreover, the specific natural environment on the TP results in unique cloud and precipitation properties, especially when compared to low-altitude regions [10,11], and can prominently limit the simulation capabilities of numerical

weather prediction models. As a kinetic factor, vertical air motion plays an important role during the formation and evolution of convective cloud processes. However, due to the rapid change and complicated dynamic structure of convective clouds, accurate and high-resolution measurements of vertical air velocity obtained by remote sensing equipment are still lacking and challenging to apply. Moreover, convective clouds over the TP have certain characteristics, such as ice phases, weaker intensities, smaller scales, and shorter life cycles, which will worsen the retrieval difficulty. In meteorological research, retrieval of vertical air velocity would help us to better understand the dynamical processes of clouds during their lifetimes, and it would promote the parameterization of physical mechanisms within models at many scales.

Millimeter-wave Doppler radar (generally dubbed "cloud radar") has been extensively developed over the last 20 years, becoming a major tool for the observation of clouds and light precipitation because of its high sensitivity and resolution. Cloud radars operate mainly in the Ka-band (~35 GHz, with a wavelength of 8 mm) and W-band (~94 GHz, with a wavelength of 3 mm), and their excellent performance in cloud detection has been demonstrated by many studies [12–16]. When an antenna is pointed vertically, cloud radar can measure the vertical motions of cloud particles in the atmosphere. However, the returned Doppler velocities consist of both particle terminal velocities and air motions [17]. Moreover, for convective clouds, radar-measured Doppler velocities can be influenced by small-scale turbulence and wind shear within the sampling volume [18]. Thus, the deviation of the vertical air velocity in convective clouds from oriented cloud radar measurements is difficult.

In several early studies, meteorologists tried to establish an explicit relationship between radar reflectivity (Z) and mean fall velocity of particles (V_t) in quiet air, because both Z and V_t are proportional to hydrometeor diameter (D). The relationship was produced by theoretical derivations and practical observations [19–22]. Using this relationship, vertical air velocity can be deduced by subtracting V_t estimated by radar-measured Z from the radar-measured mean Doppler velocity. However, the prerequisites of this method are knowledge of the particle size distribution and an accurate $V_T - D$ equation, which are complicated and currently undefined for convective ice clouds. For a received radar signal, the Fast Fourier Transform, or other spectrum analysis algorithms, can be utilized to obtain the cloud radar Doppler spectra, which contain a wealth of information about cloud properties, vertical air motion, and turbulence. Under specific sets of conditions, cloud radar spectra can provide more reliable source data for the retrieval of vertical air velocity. During strong precipitation, W-band cloud radar will suffer from Mie scattering owing to its very short wavelength, and the signature of the observed spectra (modulated by the backscattering function that oscillates between fixed maxima and minima in the Mie regime) can be used as a reference point to retrieve the air velocity.

This processing methodology was first mentioned by Lhermitte, and it has been verified and applied by Kollias to derive the updrafts and downdrafts in strong convective precipitation [18,23]. However, despite its attraction, this novel application for vertical air motion retrieval does not work under conditions of no precipitation or light precipitation for W- and Ka-band radars. When small particles, such as liquid droplets and small ice crystals, are present within the cloud radar sampling volume, vertical air velocity can be directly estimated by using the velocity bin of these small targets, and so they are regarded as tracers of clear-air motion in the measured spectra [24–27]. This methodology may be widely applied to different cloud types, but spectral broadening caused by turbulence and wind shear must be considered as non-negligible uncertainties.

In this manuscript, a technique for retrieving vertical air velocity in convective clouds over the TP is introduced. This technique is designed for a Ka-band solid-state cloud radar used in the Third Tibetan Plateau Meteorological Science Experiment (TIPEX-III). In the following section, details of the cloud radar and experiment, data processing of radar recorded Doppler spectra, and an integrated retrieval technique using three-mode Doppler spectra are described. Section 3 analyzes the retrieval results of two typical cases and compares them with another retrieved result from a ground-based

optical disdrometer. Section 4 discusses the results and the future research directions. Section 5 gives a summary and conclusions of this research.

2. Materials and Methods

2.1. Experiment, Instrument, and Measurements

In the summer of 2013, the Chinese Academy of Meteorological Sciences (CAMS) and several other research institutes launched the TIPEX-III experiment, which is the newest and largest meteorological experiment on the TP, with a duration of ten years. One purpose of this experiment is to use multi-wavelength radars, microwave radiometers, disdrometers, and other ground-based equipment to construct a three-dimensional observation system for clouds and precipitation. The first-stage mission of this experiment was achieved in the summers of 2014 and 2015 [28].

The primary instrument is a vertically pointing millimeter-wave cloud radar, deployed at Naqu in the Tibet autonomous region (latitude: $32°19'$ N; longitude: $92°04'$ E; altitude: 4507 m), to detect the vertical profiles of clouds and weak precipitation. This radar was developed by CAMS and the 23rd Institute of China Aerospace Science and Technology Corporation. To better adapt to the hostile environment of the plateau and to ensure a long-term operating capacity, the radar uses a solid-state transmitter and is equipped with an independent container. The radar operates at 33.44 GHz (a wavelength of 8.9 mm) with a peak power of over 100 W. The primary aim of using the Ka-band is to obtain as much backscattered energy as possible under the Rayleigh scattering mechanism, while reducing the attenuation effects of air and precipitation particles. A 2-m-diameter Cassegrain antenna was used to achieve a 53-dB gain and to form a 0.3-degree beamwidth, so that the radar's horizontal resolution is only 26 m at 5 km (above ground level (AGL)). The transmitted pulse width is 0.2 μs, corresponding to a vertical resolution of 30 m. Thus, the radar can provide fine-resolution mapping of cloud structures and boundaries. The radar measurements include the initial Doppler spectrum, reflectivity (Z, dBZ), mean Doppler velocity (MV, m·s^{-1}), spectrum width (σ_v, m·s^{-1}), linear depolarization ratio (LDR, dB), skewness (S_k, unitless), and kurtosis (K_t, unitless). For the Doppler spectrum, a positive velocity represents downward motion of the targets (toward to radar antenna), and negative velocity means upward motion of targets (away from radar antenna). However, for MV and retrieval of vertical air velocity (ω, m·s^{-1}), the signs are opposite. The major technical and operational parameters of the radar are summarized in Table 1.

For the radar system, the key performance indicators, such as its sensitivity, detectable range, unambiguous velocity, and velocity resolution, are a compromise. So, to meet the requirements for cloud and precipitation observation over the TP at different heights and with different intensities, three operational modes were designed for this radar: the boundary mode (BL), the cirrus mode (CI), and the precipitation mode (PR). The three modes were configured with different pulse widths and coherent and incoherent integration numbers. BL and PR are used mainly to observe clouds and light precipitation in the low and middle levels. Short pulses ensure a small blind range for both modes, while the minimum detectable reflectivity is relatively large. The major difference between BL and PR is that the BL mode performs four times more coherent integrations, which reduce the minimum detectable reflectivity by 6 dB, decrease the Nyquist velocity by a factor of 4, and increase the velocity resolution by a factor of 4. CI is used for cloud detection in the middle and upper levels, where clouds are characterized by high altitude and small or moderate reflectivity and vertical motion. For this purpose, pulse compression (with a wide pulse of 12 μs) and twice as much coherent integration are used to decrease the minimum detectable reflectivity by 20 dB. CI has a high detection range and moderate Nyquist velocity and velocity resolution, but a larger blind range from 0.12 m to 2.01 km. The radar system operates the three modes periodically, i.e., once the radial measurement is finished in one mode, the radar immediately switches to another. Each mode requires ~3 s for signal dwell and data processing, so the final temporal resolution of the radar is ~9 s. The observations collected by the

three modes are saved separately and a merging algorithm is used to produce the integrated spectral moments [28]. Operational parameters of the three modes are summarized in Table 2.

Table 1. Major technical and operational parameters of the Third Tibetan Plateau Meteorological Science Experiment (TIPEX-III) cloud radar.

Items	Technical Specifications
Radar system	Doppler, solid-state, depolarization, multi-mode
Frequency	33.44 GHz
Wavelength	8.9 mm
Transmitted peak power	≥100 W
Sensitivity	−38 dBZ at 5 km
Antenna diameter	2 m
Antenna gain	≥53 dB
Pulse width	0.2 μs, 12 μs
Beam width	0.3°
Pulse repetition frequency	8333 Hz
Range gate number	510
Detection range	Height: 150 m ~15.3 km
	Measurable reflectivity range: −50 ~30 dBZ
	Unambiguous velocity range: $-18.54 \sim +18.54$ m·s^{-1} (maximum)
Resolution	Temporal resolution: ~9 s (adjustable)
	Vertical resolution: 30 m
	horizontal resolution: 26 m at 5 km
Measurements	Original data: Doppler spectra
	Spectral moments: reflectivity (Z), mean Doppler velocity (MV), spectrum width (σ_v), linear depolarization ratio (LDR), skewness (S_k), kurtosis (K_t), etc.

Table 2. Operational parameters of three modes. BL = boundary mode; CI = cirrus mode; and PR = precipitation mode.

Parameters	Mode		
	BL	CI	PR
Detectable range (km)	0.12–7.5	2.04–15.3	0.12–12
Pulse width (μs)	0.2	12	0.2
Pulse period (μs)	120	120	120
Pulse repetition frequency (Hz)	8333	8333	8333
Number of coherent integrations	4	2	1
Number of incoherent integrations	16	32	64
Sensitivity	−24 dBZ at 5km	−38 dBZ at 5km	−18 dBZ at 5km
Spectral bin number	256	256	256
Nyquist velocity (m·s^{-1})	±4.635	±9.27	±18.54
Velocity resolution (cm·s^{-1})	3.64	7.27	14.54

To simply assess the detection capability of this radar, the probability distribution of measured reflectivity at different heights, collected from June to August 2014 and July to September 2015, was calculated. As shown in Figure 1, the realistic minimum detectable reflectivities of BL and CI at

different heights are coincident with the theoretical results (marked curves), indicating that they met expectations for weak cloud observation. CI has a 20 dB and a 14 dB weaker minimum detectable reflectivity than PR and BL, respectively. However, strong reflectivity, greater than 30 dBZ, was rarely observed due to signal attenuation and Mie scattering at this wavelength. Zheng investigated the measurement deviation of this radar by comparing it with a C-band vertically pointing radar and suggested that a 2 dB bias may exist under light precipitating conditions, with a maximum reflectivity of no more than 27 dBZ [29]. Figure 2 presents an example of 3-h time-height cross-sections of reflectivity from the three different modes made on 20 July 2015. It demonstrates that CI can detect much weaker reflectivity in the cloud boundary than can BL and PR, at heights above 2.01 km. Some artifacts were caused by the pulse compression on the cloud top or under the cloud base. Two layers of cirrus clouds can be clearly observed in the CI map, but are obscured in the BL and PR maps. BL is more appropriate than PR for weak cloud observation (see the small-scale cumulus near 1 km) below 2.01 km. PR, on the other hand, is more suitable than BL for light precipitation observation.
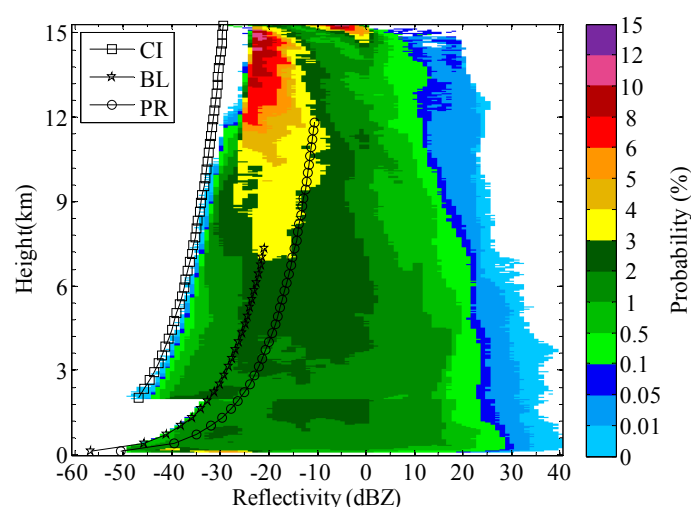

Figure 1. Statistical probability distribution of radar-measured reflectivity at different heights, collected over the Tibetan Plateau (TP) from June to August 2014 and July to September 2015. The spectrogram illustrates the radar's actual detection capability for weak and strong meteorological targets, and the marked curves represent the theoretical sensitivities of three operational modes. In the figure, CI, BL, and PR represent cirrus mode, boundary mode, and precipitation mode, respectively.

2.2. Data Processing of Cloud Radar Doppler Spectra

The TIPEX-III cloud radar produces vertically resolved measurements of Doppler spectra, which consist of 256 spectral bins and represent the distribution of returned radar power as a function of hydrometer radial velocity in the sampling volume. Cloud radar Doppler spectra have been commonly used for cloud property retrieval and microphysical studies because of their wealth of information on drop size distribution, turbulence, vertical air motion, and so on. However, Doppler spectra simultaneously contain radar noise and meteorological signals, and they suffer from velocity aliasing under special conditions. To minimize these effects before further application, data processing procedures were performed, as presented here.

First, a 3-point boxcar averaging window was used to smooth all Doppler spectra to improve spectral clarity and decrease the fluctuation of radar noise. Noise level calculation was a crucial step to accurately separate the radar noise and cloud signal. An objective method presented by Hildebrand and Sekhon has been commonly used for millimeter-wave cloud radar studies [18,26,30,31]. However, a recent study argues that this approach can overestimate the radar noise power and so is not appropriate for solid-state cloud radars. In contrast, a segmental approach reported by Petitdidier et al. can achieve better accuracy and stability [29,32]. So, in this study, a simple 8-segment technology

was utilized to calculate radar noise level. Spectra were divided into eight segments, with the lowest integrated power segment regarded as the range that was dominated by radar noise, without any meteorological signal. The mean power of this segment was calculated as the noise level for the whole Doppler spectrum. Subsequently, all continuous spectral bins above the noise level were picked and further judged by a Signal-to-Noise Ratio (SNR) threshold and a bin-number threshold, since cloud signal typically has a higher power and larger spectral width than the noise level. Only the consecutive signals with the first three powers were reserved, and several spectral parameters, such as SNRs, left endpoints, right endpoints, and peaks, were also recorded.
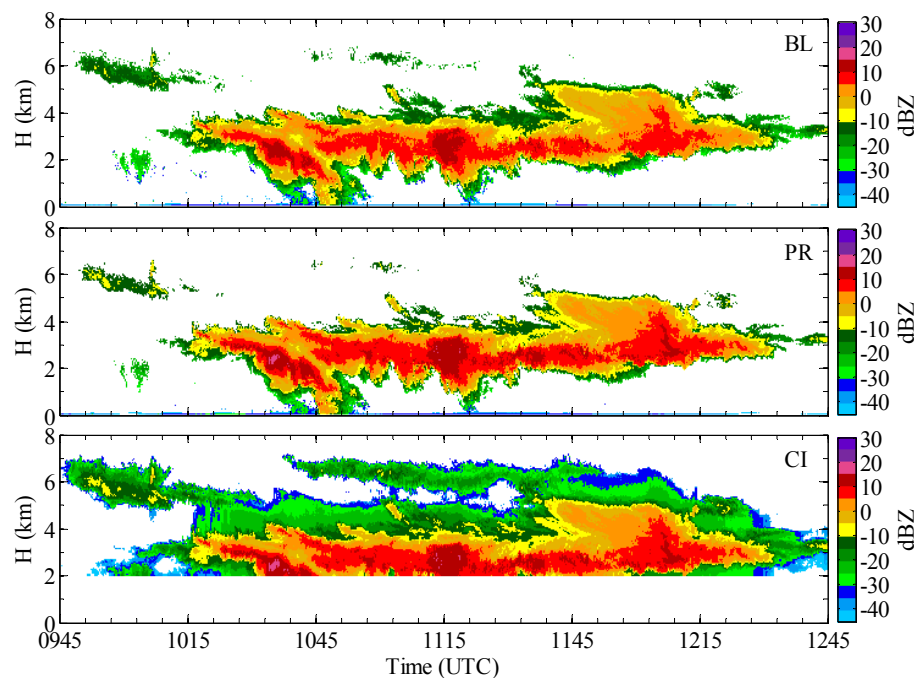

Figure 2. An example of 3-h time-height cross-sections of reflectivity from all three operational modes observed on 20 July 2015. In the figure, CI, BL, and PR are cirrus mode, boundary mode, and precipitation mode, respectively.

Due to more coherent integration numbers being used, radar BL and CI modes obtained relatively small measurable velocity ranges from -4.635 to $4.635\,\mathrm{m\cdot s^{-1}}$ and from -9.27 to $9.27\,\mathrm{m\cdot s^{-1}}$, respectively. In the presence of large droplets or strong airflows in convective systems, the measured Doppler spectra may be folded, which leads not only to discontinuity of the cloud signal, but also to spectral moments (such as MV and σ_v) that generate significant errors. Here, a previously presented algorithm was used for velocity dealiasing of Doppler spectra [29]. This algorithm can iteratively judge and correct the folded Doppler spectra from cloud top to base and can automatically determine the folding type, a property that is caused by either rapid hydrometer sinking or a strong updraft in the interior of the convective system. After the ambiguous Doppler spectra were corrected, the corresponding spectral parameters were also readjusted. BL and CI Doppler spectra, collected from TIPEX-III in the summers of 2014 and 2015, were used for assessing the dealiasing effects, by comparison with the corresponding spectra of the PR mode. Results show a success rate of 99.8% when this algorithm was used in only a one-time fold.

Figure 3 shows a typical case of a convective cloud, collected at 10:00 UTC on 5 July 2014, by the CI mode. From the mapping of the original spectra (Figure 3a), parts of the ambiguous signal can be found near 6 km, due to strong updraft. Parts of the ambiguous signal also exist below 4.3 km, because of rapid fall speeds of ice crystals and raindrops. After dealiasing (Figure 3b), these two ambiguous signal parts were identified and corrected, so that the upper one is shifted to the left

terminal and the lower one is shifted to the right terminal. Two profiles of the MV were calculated from the original and the corrected spectra (Figure 3c), showing one maximum deviation approaching $4 \text{ m} \cdot \text{s}^{-1}$ at 6 km and another of $-6 \text{ m} \cdot \text{s}^{-1}$ at 3.4 km. Meanwhile, two profiles of the estimated σ_v presented more serious deviations in the spectral folded regions, with a maximum bias of $4.5 \text{ m} \cdot \text{s}^{-1}$ at 6 km and another maximum bias of $7.5 \text{ m} \cdot \text{s}^{-1}$ at 3.4 km.
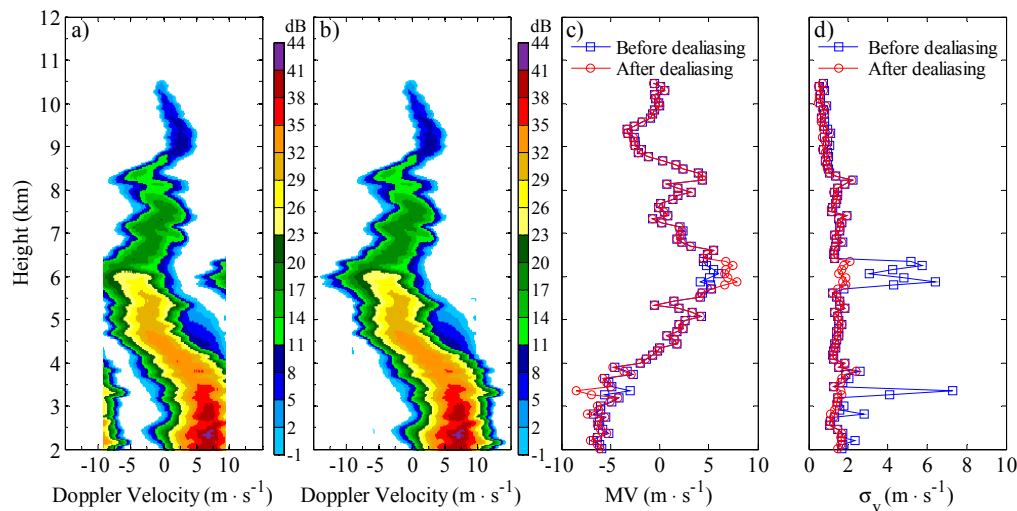

Figure 3. A velocity dealiasing case made from a convective cloud collected at 10:00 UTC on 5 July 2014 by CI mode; (**a**) is the original Doppler spectra at different heights; (**b**) is the corresponding corrected spectra after dealiasing; (**c**) is the estimated MV from (**a**,**b**); and (**d**) is the σ_v estimated from (**a**,**b**). The power of Doppler spectra denoted by dB, which represents an analog-to-digital (A/D) converter count and can be converted to dBm by $10 \times log_{10}$ dB minus the radar receiver gain.

2.3. Retrieval Method

2.3.1. Essential Idea

The Doppler velocities of a cloud signal in the resolved spectra are typically proportional to the hydrometeor diameters, based on the assumption that they experience uniform vertical air motion and homogeneous turbulence in the radar sampling volume. Thus, the left spectral edge of an identified cloud signal should be generated by the smallest cloud particles. Because of the limited size of these small targets, their corresponding fall speed will be negligible when compared with that of the active vertical air motions in a convective cloud on the TP, which are one or two orders of magnitude larger. As a result, we can directly derive the vertical air velocity by using the left spectral bin, which regards the smallest cloud particles as a tracer of clear-air motions. This simple idea (here referred to as the "small-particle-traced idea") was previously described by Gossard and Kollias and then further validated by Shupe [24–26]. Figure 4 shows a schematic of the small-particle-traced idea, where the $\omega_{initial}$ represents the initial estimate of the vertical air velocity.

2.3.2. Integrated Retrieval Technique Using Multimode Doppler Spectra

To effectively use the Doppler spectra from the TIPEX-III cloud radar for retrieving vertical air motions in convective clouds, the following three aspects require further consideration:

(1) The three operational modes have different sensitivities, detectable height ranges, Nyquist velocities, and spectral velocity resolutions. These key performance parameters are crucial for the estimation of vertical air velocity. Thus, comprehensive usage of the multimode data needs to be considered to obtain more reasonable and accurate results.

(2) Convective clouds over the TP commonly vary rapidly with small scales, and, thus, the measured radar Doppler spectra in a sampling volume can be broadened by the active turbulence, wind shear, and inhomogeneous horizontal wind, which will cause bias to the retrieval results. Therefore, spectral broadening needs to be further revised.

(3) Because of a low melting layer altitude of approximately 1 km on the TP, hydrometeors in the interior of convective cells exist mostly in the ice phase, which typically involves greater diameters than the liquid phase. Furthermore, the rain droplets under the cloud base also have relatively large diameters. Therefore, as the fall velocities of the traced targets in the radar sampling volume cannot be neglected, the possible biases that this introduces to the small-particle-traced idea need to be documented.
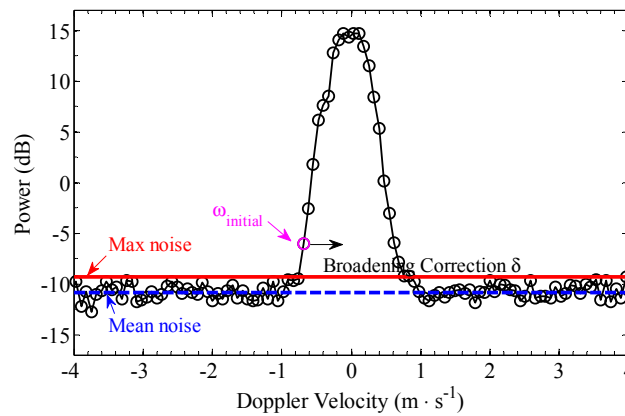

Figure 4. Schematic of the small-particle-traced idea. The blue dashed line is the estimated radar mean noise, the solid red line is the max noise, the ω_{initial} represents the initial retrieval of vertical air velocity.

Based on these three considerations, an integrated technique using multimode Doppler spectra is proposed for comprehensive retrieval of vertical air velocity. Figure 5 shows a flow diagram of the method. For the height range 2.01–15.3 km, Doppler spectra from CI are used, because this mode is more sensitive at detecting smaller cloud targets and has a higher detectable range. For the height range below 2.01 km (0.12–1.98 km), Z is utilized to judge whether BL or PR would be more appropriate for the retrieval. If Z is greater than -10 dBZ or the echo base has approached the near-ground level, then Doppler spectra of PR are selected, because the measurements correspond to a relatively strong or precipitating cloud and PR has a wider velocity range and a robust dynamic range. However, if Z is lower than -10 dBZ and the echo base is above the near-ground, then the measurements correspond to a relatively weak cloud, and Doppler spectra of BL are chosen because of their higher velocity resolution and better sensitivity. After data selection, ω can be derived from the three modes by the small-particle-traced idea and its necessary data processing.

Under actual conditions, radar-measured spectra are broader than expected from the cloud particle size distribution alone because of the temporal and spatial filters that introduce additional broadening. The Doppler spectrum variance for a vertically pointing radar can be written as [27]

$$\sigma_v^2 = \sigma_{\text{DSD}}^2 + \sigma_T^2 + \sigma_S^2 + \sigma_B^2 \tag{1}$$

where σ_{DSD}^2 is the variance induced by the particle size distribution, σ_T^2 is the variance caused by turbulence, σ_S^2 is the variance due to wind shear, and σ_B^2 is the variance introduced by a finite radar beamwidth. For retrieval of vertical air velocity from an observed Doppler spectrum, without the knowledge of σ_{DSD}^2, the latter three terms are used to correct for the effects of the broadening of the left edge of the spectrum due to non-hydrometeor size distribution.
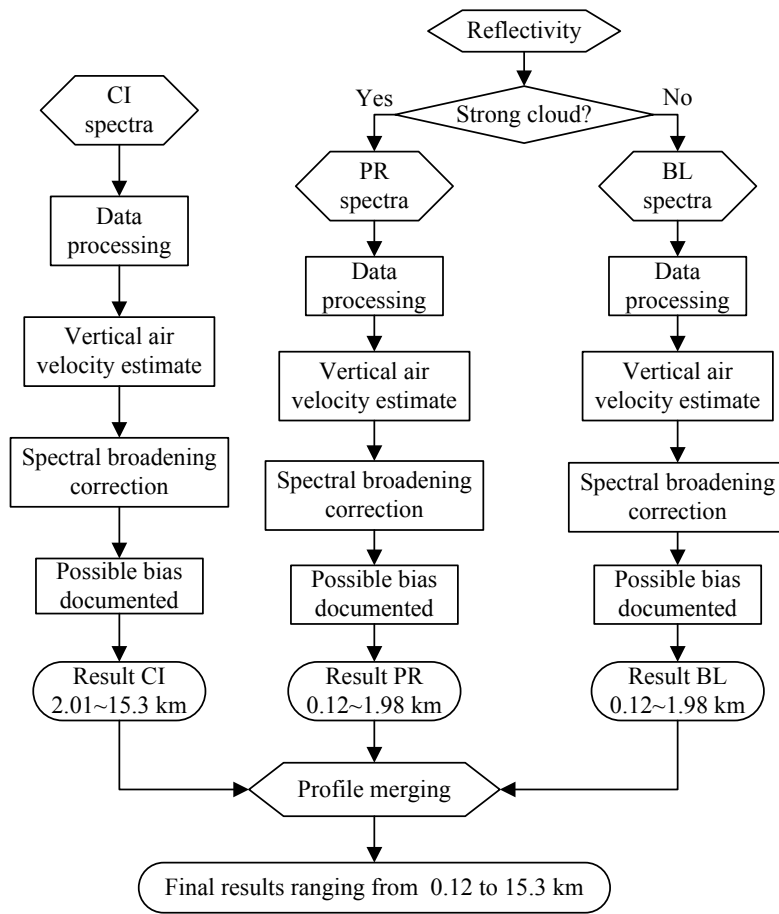
Figure 5. Flow diagram of the integrated technique for retrieval of vertical air velocity using multimode Doppler spectra.

For a symmetric Gaussian antenna, σ_B^2 can be estimated by using the horizontal wind speed, U (m·s^{-1}, obtained by radiosonde), and the radar beamwidth (θ) [17] as follows:

$$\sigma_B^2 = \frac{U^2 \theta^2}{2.76^2} \tag{2}$$

σ_S^2 is caused by vertical (k_h) and horizontal (k_v) shear in the vertical winds (both in s^{-1}), and this term can be estimated from Equation (3) [17,25,26]. The first term represents transverse shear and the second term represents radial shear. R is the distance from the target to the radar, Δ is the radar gate length, and both k_h and k_v can be calculated by the MV across three adjacent points.

$$\sigma_S^2 = \frac{k_h^2 R^2 \theta^2}{2.766^2} + \frac{k_v^2 \Delta^2}{12} \tag{3}$$

Turbulent broadening of the spectrum variance can be derived by using the temporal variance of the measured mean Doppler velocity, σ_{vm}^2, with the assumption that the length scales of the turbulent eddies observed by the radar are within the inertial subrange of the turbulence spectrum [33,34]. The σ_{vm}^2 can be calculated as follows:

$$\sigma_{vm}^2 = \frac{\sum_{i=-n/2}^{i=n/2} \left(MV_i - \overline{MV} \right)^2}{n} \tag{4}$$

where n is the adjacent gate number (here set to 7, as the turbulence length scales are assumed to be mostly within 60 s of the radar observational time), MV_i represents the mean Doppler velocity of each gate, and $\overline{MV}$ is the overall average. O'Connor et al. (2005) showed that the relationship between σ_T^2 and σ_{vm}^2 can be described by a simple form:

$$\frac{\sigma_T^2}{\sigma_{vm}^2} = \frac{L_s^{2/3}}{L_l^{2/3} - L_s^{2/3}} \tag{5}$$

In Equation (5), L_s is the horizontal length of the radar sampling volume for a 2 s dwell time and L_l represents the larger eddies passing through the effective sampling volume that results from an average of the radar observations over 60 s [27]. L_s and L_l can both be given as $L = Ut + 2R\sin(\theta/2)$, where t is the observation time.

After estimating these three spectral broadening components, a correction factor δ (m·s^{-1}) can be calculated, by which the initial air velocity $\omega_{initial}$ is increased in the direction of the arrow in Figure 4. δ can be written as

$$\delta = \sigma_v - \sqrt{\sigma_v^2 - \left(\sigma_T^2 + \sigma_S^2 + \sigma_B^2\right)} \tag{6}$$

For relatively strong convective clouds or light precipitation, the smallest traced targets in the radar sampling volume may possibly have non-negligible sizes, corresponding to terminal speeds that affect the accuracy of the derived air velocities. However, these retrieval biases are difficult to estimate because the particles in convective clouds on the TP have unresolved phases or habits.

As a simple solution, reflectivity of the traced spectral bin (similar to Z), Z_{traced} (in dBZ), can be calculated to document the qualitative reliability and bias of the retrieval. The value of Z_{traced} is related to the size of the traced target, which can be used to judge whether the terminal speed could be neglected. A small value of Z_{traced} can illustrate that the traced target is small-sized, with a negligible terminal speed, and the retrieved ω from Doppler spectra will be reliable and accurate. On the contrary, a large value of Z_{traced} can indicate that the traced target is relatively large, with a non-negligible terminal speed; as a result, the retrieved ω will have a certain bias.

After the above processing, a simple procedure is performed to merge the results from three modes. The procedure uses the deviation between the CI and BL/PR to shift the profile under 2.01 km, since CI (corresponding to the upper profile with a range from 2.01 to 15.3 km) wields the best sensitivity, which is useful for maintaining retrieval accuracy. Finally, an entire profile with a range from 0.12 to 15.3 km is obtained.

3. Results

3.1. Two Typical Cases

Various types of convective clouds frequently occur in the summertime on the TP. Under different synoptic conditions, the clouds may have different macro and micro properties. The two typical cases selected below were used to study the characteristics of cloud processes and vertical air motions.

The first case is a series of fair-weather shallow cumuli collected from 19:00 to 21:30 UTC on 16 July 2015, during a typical convection process induced by a weak unstable atmosphere caused by daytime surface heating, with no synoptic system. The 2.5 h cloud radar measurements and retrievals are shown in Figure 6. From the mapping, a series of small-scale cumuli are found at 2–3 km with a reflectivity range from −30 to 5 dBZ. An alternating variation was observed in radar-measured Z, MV, and σ_v across the cumuli, thus indicating that inhomogeneous ω and microscopic properties were being generated in the interior of the clouds, a feature that is strikingly similar to aircraft observations from previous studies [35]. As expected, the derived vertical air velocities show updrafts that occur in the middle of cumulous cells with the cores corresponding to positive MV and downdrafts located on both sides. Figure 7 shows the curves of the height-averaged results of Z, σ_v, and ω. It indicates that the general trends of ω and Z are similar: the updrafts are associated with high cloud radar Z,

and the downdrafts are correlated with low Z. The cloud-inner updrafts can be produced by both environmental upflow and potential heating, with an average speed of 1 m·s^{-1}, and the downdrafts can be caused by mixing of the environmental air at cloud top and evaporative cooling, with an average speed of -0.3 m·s^{-1}. Spectrum widths less than 0.25 m·s^{-1} are observed in the updraft areas, suggesting less turbulent flow associated with relatively weak horizontal variability of vertical air motions and a gradual vertically accelerating motion. However, at the edges of the updraft, the σ_v increased to about 0.25–0.3 m·s^{-1}, particularly in the narrow areas between the updrafts and downdrafts. This broadening of the spectra may be due to sharp horizontal gradients in the vertical wind. As seen in Figure 6, the intensity of the smallest traced targets (Z_{traced}) is low, with a range from -48 to -33 dBZ. This demonstrates that the retrieval results can be quite accurate, with a negligible particle terminal speed when compared with the motion of the air itself.
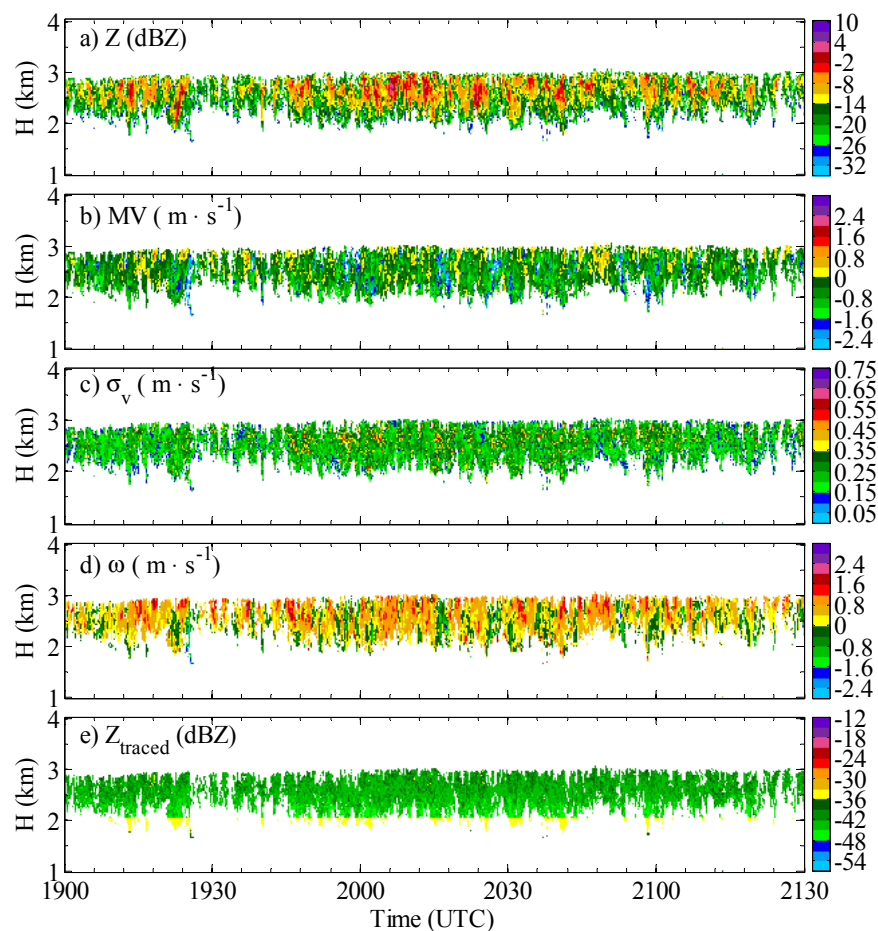

Figure 6. Cloud radar measurements and retrieval results of a series of fair-weather shallow cumuli collected from 19:00 to 21:30 UTC on 16 July 2015; (**a**) is the reflectivity; (**b**) is the mean Doppler velocity; (**c**) is the spectrum width; (**d**) is the vertical air velocity; (**e**) is the reflectivity of traced spectral bin.
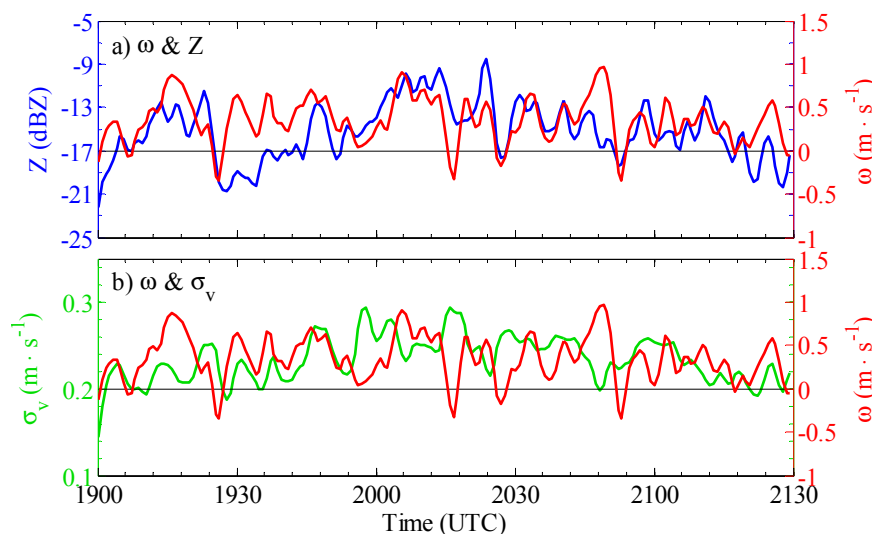
Figure 7. Height-average curves of the Z (blue curve), σ_v (green curve), and ω (red curve); (**a**) is the changing curves of ω and Z; (**b**) is the changing curves of ω and σ_v.

The second case is a light convective precipitation process collected from 13:40 to 19:00 UTC on 18 August 2015, under the synoptic condition of a plateau shear line, which can be found clearly over the 500 hPa weather chart (not shown). The 5.2 h radar measurements and retrievals of cloud and precipitation are shown in Figure 8. The Z mapping illustrates that there are seven different convective clouds (marked as A, B, C, D, E, F, and G) that pass over the radar site during the observation period. Of these, C is a layer of cirrostratus clouds located at 7 to 10.5 km, with a reflectivity range from -5 to 15 dBZ, while the others are precipitating cumulonimbus clouds with a maximum Z of over 25 dBZ. A and B are stronger and deeper than D, E, and F, with top heights near 4.5 km and 7 km, respectively. D, E, and F have 3–4 km cloud tops. The derived vertical air velocities indicate that the updrafts appear in the upper half of the convective cells, with strong cores corresponding to positive MV. The air velocities gradually accelerate from cloud middle to cloud top, and they may be intimately related to the development level of cumulonimbus, and stronger updrafts are relevant to the deeper cloud body. The lower halves of the cirrostratus and cumulonimbus clouds are both dominated by downdrafts, with a few weak updrafts. As a result, a melting layer near 1.3 km can be found with sudden increases of MV and σ_v. Figure 9 presents 1.5–6 km average curves of Z, ω, σ_v, and raindrop size distribution on the ground collected by a disdrometer. It suggests that the ω follows similar trends to the cloud Z and σ_v. The updrafts promote the formation of large ice crystals in the interior of the cloud, inducing the increases in Z and wider Doppler spectra. This may be different from case one, in which the higher σ_v values are mostly caused by inhomogeneous and small-scale variations of the vertical air motions. The raindrop size distribution also exhibits a high correlation with vertical air motion, as larger raindrops appear in response to updrafts after a few minutes of delay, such as in cloud B, where the three bursts of larger raindrops are related to the three gusts of updrafts. As seen in Figure 8, the intensities of the smallest traced targets imply that the retrievals above 2.01 km from the CI mode may be relatively accurate with a range from -48 to -30 dBZ, while the results below 2.01 km derived from the PR or BL modes will suffer from a larger bias. Thus, the amendment and merging in our retrieval technique are both necessary and beneficial.
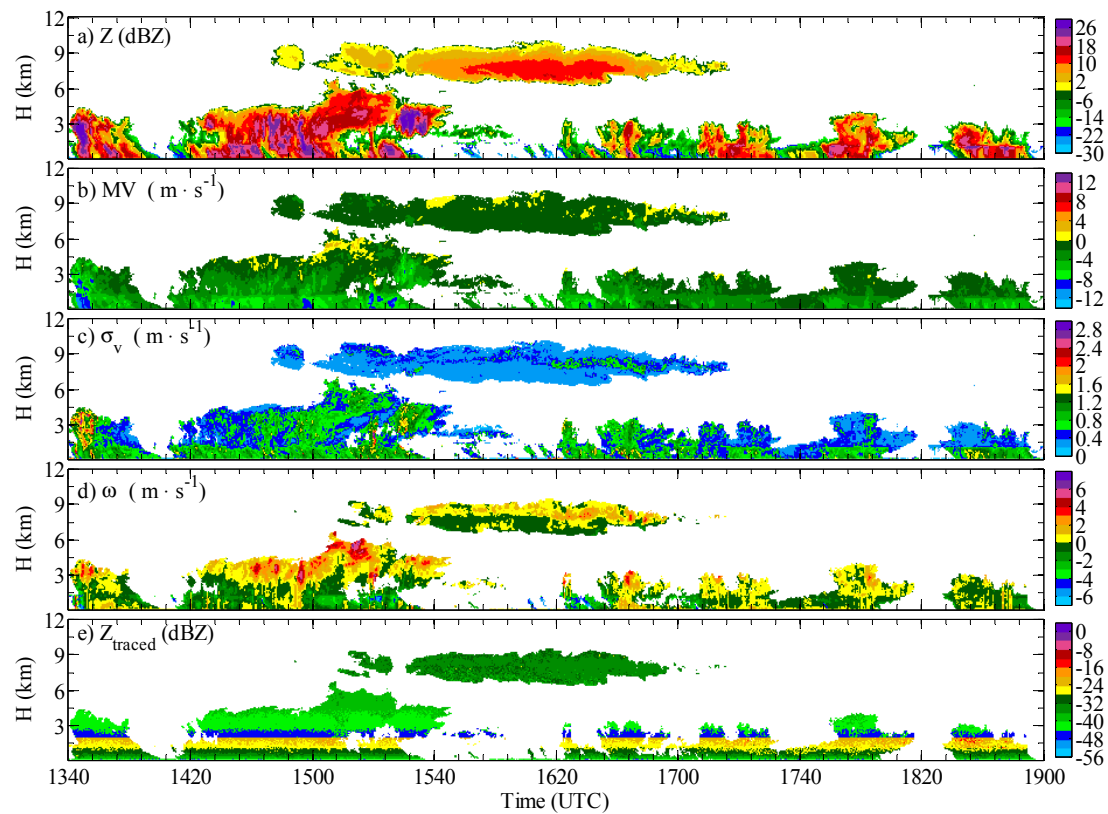
Figure 8. Cloud radar measurements and retrieval results of a light convective precipitation process collected from 13:40 to 19:00 UTC on 18 August 2015; (**a**) is the reflectivity; (**b**) is the mean Doppler velocity; (**c**) is the spectrum width; (**d**) is the vertical air velocity; (**e**) is the reflectivity of traced spectral bin.
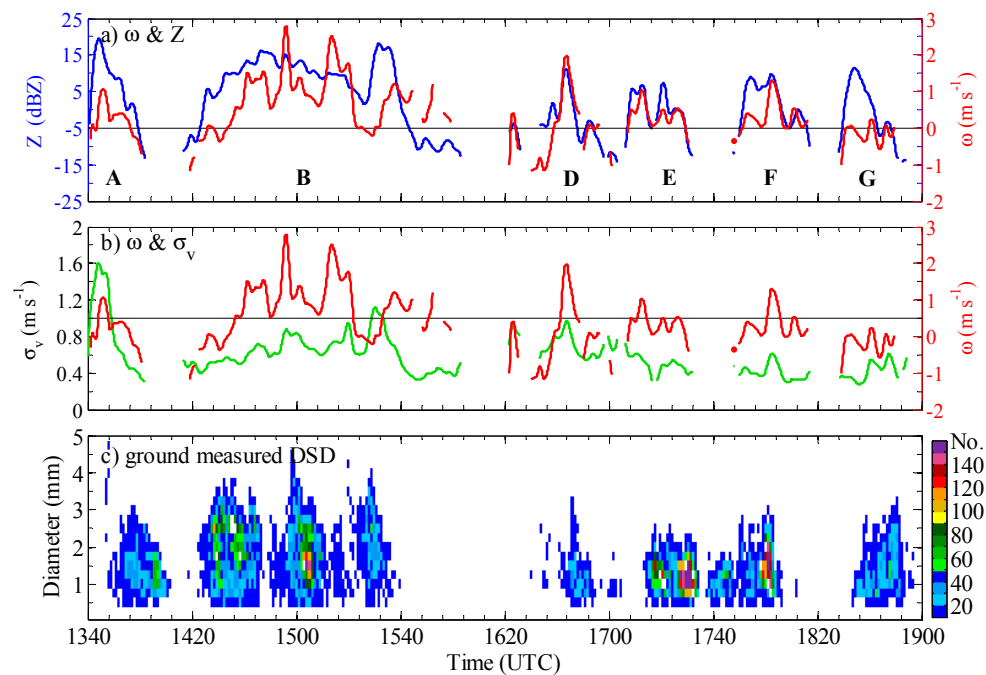

Figure 9. The 1.5–6 km average curves of the Z (blue curve), σ_v (green curve), ω (red curve), and the raindrop size distribution on the ground; (**a**) is the changing curves of ω and Z; (**b**) is the changing curves of ω and σ_v; (**c**) is the raindrop size distribution measured on the ground.

3.2. Comparing ω with Retrieval Resulst from a Disdrometer

To preliminarily validate the reliability of radar-derived vertical air velocities, indirect retrieval results from a ground-based optical disdrometer were used for comparison.

The disdrometer can simultaneously detect the equivalent diameter (D), concentration (N), and MV of raindrops near the ground (1.4 m above the surface) with a 1 min temporal resolution. With the knowledge of raindrop terminal speed (V_T), the ω can be simply inferred by subtracting V_T from MV. For liquid raindrops, many previous studies have indicated that a relationship between V_T and D can be established using an exponential function [36,37]:

$$V_T = (9.65 - 10.3 \times \exp(-0.6 \times D))/f \tag{7}$$

where f is a correction factor related to the atmospheric density. Figure 10 shows the frequency distribution of D and MV of the observed raindrops, collected from 15 July to 30 August 2015, under weak precipitating conditions ($10 \leq Z \leq 25$ dBZ). A fitting equation with a correction factor of 0.7338 can represent the $V_T - D$ relationship of the raindrop on the surface of the TP. In the mapping, the measured MV is marked by a color block, and the deviation between MV and V_T is induced by ω. From the above, the ω derived from the disdrometer can be used for comparison with the radar-derived results.
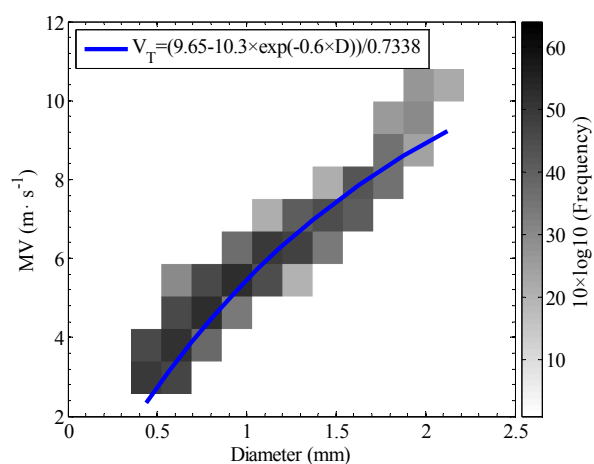

Figure 10. Frequency distribution of diameter (D) and MV of the observed raindrops collected from 15 July to 30 August 2015 under weak precipitating conditions. The blue solid line represents a fitting equation for the $V_T - D$ relationship.

Figure 11 shows the time series of retrievals from two instruments for case two, where the radar retrievals are selected from the first detectable ranging gate (150 m above the surface). The comparison illustrates that the trends of the two retrievals are basically similar, with the appearances of the updrafts or downdrafts mostly coinciding. However, the radar may have a larger fluctuation due to its high temporal resolution, and the value of the two series include certain deviations, with a mean bias of nearly 0.5 m·s^{-1}.

There are several reasons for the retrieval deviations between the two instruments. First, the cloud radar minimum detectable height is 150 m, but the disdrometer collects data only near the ground (1.4 m height), which means that the radar retrievals are located higher than that of the disdrometer's (although they are deployed co-located). Thus, two different vertical air flows are retrieved, and naturally the retrieved values will be different, as the air flow in convective cells can be changed rapidly on small scales. Second, the retrieval method for the disdrometer has some uncertainties which will affect the comparison. The most crucial uncertainty is the assumed relationship between the falling speed of particles (V_T) and their diameters (D). The "$V_T - D$" relationship will be relatively

more reliable for moderate raindrops (liquid), yet for ice hydrometeors, the "$V_T - D$" relationship is complicated and less reliable. On the TP, environmental temperatures are relatively low, which will, therefore, complicate retrievals in ice precipitation. Third, the disdrometer is two-dimensional and cannot distinguish multiple droplets when they pass through the sensor in parallel, which will also affect the retrieval results.
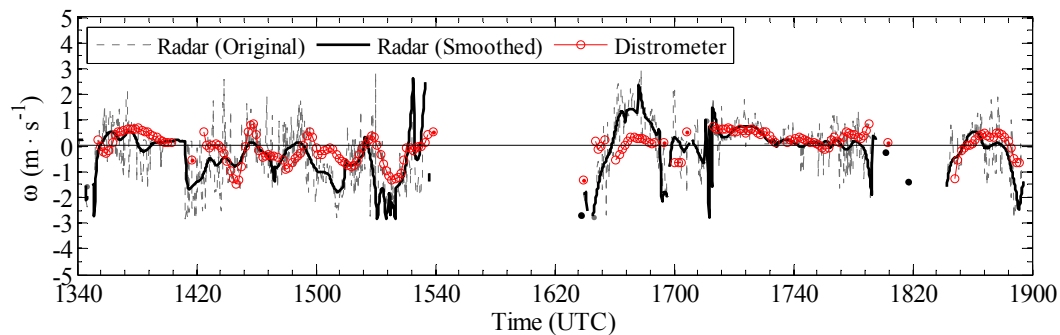

Figure 11. The time series of vertical air velocities derived by radar and disdrometer near the ground for case two, the radar retrievals are selected from the first detectable range gate at 150 m above the surface.

4. Discussion

Because of the complicated structure and relatively low magnitude of vertical air motion in convective clouds, direct measurement of accurate vertical air velocity with high resolution is difficult and still lacking. In some previous studies, observations from in-situ research aircraft were used to validate radar retrieval as a feasible solution [22,26]. However, this approach may be not work on the TP due to bad flight conditions in synoptic storms and in the presence of stronger convective cells, and also due to the low availability of airports. In this paper, the validations for radar retrievals were preliminarily performed from two aspects. First, characteristics of the other radar measurements from two cases were analyzed to qualitatively infer the reliability of the derived vertical air velocities; such as, positive mean Doppler velocities corresponding to strong updraft regions. A feature of the alternating variation of vertical air motion across the small-scale cumuli was similar to previous studies [25,35], and a melting layer was found when downdrafts predominated. These features support the use of radar retrievals for this application. Second, a surface retrieval from an optical disdrometer was formed and compared to the radar retrievals. While certain biases remain, the comparison reveals a similar trend in the vertical air velocities from the two instruments.

In the future, measurements or retrievals from other equipment (such as, wind profile radar) could be compared with cloud radar retrievals under some special conditions. However, this is just an initial idea, and further research is required.

5. Conclusions

Due to large dynamic and thermal effects, convective cells frequently occur on the TP in the summertime. Measurements of vertical air motion are useful for advancing our understanding of the dynamic and microphysical mechanisms of clouds, and they can be used to improve the parameterization of current numerical models at many scales. In this paper, a technique was presented for retrieving the high-resolution vertical air velocity in convective clouds over the TP by using vertically pointing Ka-band cloud radar. This technique further develops the small-particle-traced method and is based on the use of recorded Doppler spectra from radar and its necessary data processing, over three different modes. Spectral broadening corrections, uncertainty estimations, and results merging were used to ensure more accurate results.

Qualitative analysis of two typical convective cases showed that the retrievals of vertical air velocities were reasonable. Meanwhile, some observational features were also found. For small-scale shallow cumuli, air velocities alternately changed across the cumuli, updrafts appeared in the middle of cumulus cells, and downdrafts were located on both sides. For precipitating cumulonimbus clouds, updrafts mostly appeared in the upper half of the convective cells and gradually accelerated from cloud middle to cloud top, whereas the lower half of the cumulonimbus was dominated by downdrafts. Vertical air velocity could be intimately related to the development level of the cumulonimbus, with stronger updrafts corresponding to deeper cloud body. Quantitative retrieval of vertical air motion from a ground-based optical disdrometer was used to preliminarily validate the radar-derived results. The comparison illustrated that the trends of the two retrievals were similar, with the updraft or downdraft appearances coinciding. Cloud radar had much higher resolution retrieval results and could reveal the small-scale variation of vertical air motion. However, we noted that the different heights of the two retrievals and the uncertainty in the disdrometer-derived results, likely impacted this comparison.

Author Contributions: Jiafeng Zheng conceived, designed, processed, analyzed, and wrote the manuscript; Liping Liu and Keyun Zhu conducted the literature review; Jingya Wu and Binyun Wang processed the data used in this manuscript.

Conflicts of Interest: The authors declare no conflict of interest.

References

1. Flohn, H. Contributions to a meteorology of the Tibetan highland. In *Atmospheric Science Paper*; Colorado State University: Fort Collins, CO, USA, 1968.
2. Ye, D.Z.; Gao, Y.X. *Tibetan Plateau Meteorology*; Science Press: Beijing, China, 1979; pp. 74–79. (In Chinese)
3. Zhu, G.F.; Chen, S.J. Convective activities over the Qinghai-Xizang Plateau and adjacent regions in summer of 1995. *Plateau Meteorol.* **1999**, *18*, 9–19. (In Chinese)
4. Xu, X.D.; Zhao, T.L.; Lu, C.G.; Shi, X.H. Characteristics of the water cycle in the atmosphere over the Tibetan Plateau. *Acta Meteorol. Sin.* **2014**, *72*, 1079–1095. (In Chinese)
5. Wu, G.X.; He, B.; Liu, Q.M.; Bao, Q.; Ren, R.C. Recent progressed on dynamics of the Tibetan Plateau and Asian summer monsoon. *Chin. J. Atmos. Sci.* **2016**, *40*, 22–32. (In Chinese)
6. Qian, Z.G.; Wu, T.W.; Lv, S.H.; Jiao, Y.J. Numerical simulation of northwest China arid climate formation-effects of the Qinghai-Xizang plateau terrain and circulation field. *Chin. J. Atmos. Sci.* **1998**, *22*, 753–762. (In Chinese)
7. Jiang, J.X.; Fan, M.Z. Convective clouds and mesoscale convective systems over the Tibetan Plateau in summer. *Chin. J. Atmos. Sci.* **2002**, *26*, 263–270. (In Chinese)
8. Tao, S.Y.; Ding, Y.H. Observational evidence of the influence of the Qinghai-Xizang (Tibet) plateau on the occurrence of heavy rain and severe convective storms in China. *Bull. Am. Meteorol. Soc.* **1981**, *62*, 23–30. [CrossRef]
9. Xu, X.D.; Zhou, M.X.; Chen, J.Y. Thermal and dynamic integrated physical images of land-atmosphere over the Tibetan Plateau. *Sci. China Ser. D* **2001**, *31*, 428–440. (In Chinese)
10. Liu, L.P.; Zheng, J.F.; Ruan, Z. Comprehensive radar observations of clouds and precipitation over the Tibetan Plateau and Preliminary analysis of cloud properties. *J. Meteorol. Res.* **2015**, *29*, 546–561. [CrossRef]
11. Wang, C.H.; Shi, H.X.; Hu, H.L.; Wang, Y.; Xi, B. Properties of cloud and precipitation over the Tibetan Plateau. *Adv. Atmos. Sci.* **2015**, *32*, 1504–1516. [CrossRef]
12. Lhermitte, R. Attenuation and scattering of millimeter wavelength radiation by clouds and precipitation. *J. Atmos. Ocean. Technol.* **1990**, *7*, 464–479. [CrossRef]
13. Clothiaux, E.E.; Miller, M.A.; Albrecht, B.A.; Ackerman, T.P.; Verlinde, J.; Babb, D.M.; Peters, R.; Syrett, W.J. An evaluation of a 94-GHz radar for remote sensing of cloud properties. *J. Atmos. Ocean. Technol.* **1995**, *12*, 201–229. [CrossRef]

14. Kollias, P.; Clothiaux, E.; Miller, M.; Albrecht, B.; Ackerman, G.T. Millimeter-wavelength radars: New frontier in atmospheric cloud and precipitation research. *Bull. Am. Meteorol. Soc.* **2007**, *88*, 1608–1624. [CrossRef]

15. Illingworth, A.J.; Hogan, R.J.; O'connor, E.J.; Bouniol, D.; Delanoë, J.; Pelon, J.; Protat, A.; Brooks, M.E.; Gaussiat, N.; Wilson, D.R.; et al. Cloudnet: Continuous evaluation of cloud profiles in seven operational models using ground-based observations. *Bull. Am. Meteorol. Soc.* **2007**, *88*, 883–898. [CrossRef]

16. Ulrich, G.; Volker, L.; Matthias, B.; Gerhard, P.; Dmytro, V.; Vladimir, V.; Vadim, V. A 35-GHz polarimetric Doppler radar for long-term observations of cloud parameters—Description of system and data processing. *J. Atmos. Ocean. Technol.* **2015**, *32*, 675–690.

17. Gossard, E.E.; Strauch, R.G. *Radar Observations of Clear Air and Clouds*; Elsevier: New York, NY, USA, 1983; p. 280.

18. Kollias, P.; Albrecht, B.A.; Marks, F.D., Jr. Cloud radar observations of vertical drafts and microphysics in convective rain. *J. Geophys. Res.* **2003**, *108*, 40–53. [CrossRef]

19. Rogers, R.R. An extension of the Z-R relation for Doppler radars. In Proceedings of the 11th Weather Radar Conference AMS, Boston, MA, USA, 14–18 Spetember 1964.

20. Sekhon, R.S.; Srivastava, R.C. Doppler radar observations of drop-size distribution in a thunderstorm. *J. Atmos. Sci.* **1971**, *28*, 983–994. [CrossRef]

21. Hauser, D.; Amayenc, P. A new method for deducing hydrometeor-size distributions and vertical air motions from Doppler radar measurements at vertical incidence. *J. Appl. Meteorol.* **1981**, *20*, 547–555. [CrossRef]

22. Giangrande, S.E.; Collis, S.; Straka, J. A summary of convective-core vertical velocity properties using ARM UHF wind profilers in Oklahoma. *J. Appl. Meteorol. Climatol.* **2013**, *52*, 2278–2295. [CrossRef]

23. Lhermitte, R. Observations of rain at vertical incidence with a 94 GHz Doppler radar: An insight of Mie scattering. *Geophys. Res. Lett.* **1988**, *15*, 1125–1128. [CrossRef]

24. Gossard, E.E. Measurement of cloud droplet size spectra by Doppler radar. *J. Atmos. Ocean. Technol.* **1994**, *11*, 712–726. [CrossRef]

25. Kollias, P.; Albrecht, B.A.; Lhermitte, R.; Savtchenko, A. Radar observations of updrafts, downdrafts, and turbulence in fair weather cumuli. *J. Atmos. Sci.* **2001**, *58*, 1750–1766. [CrossRef]

26. Shupe, M.D.; Kollias, P.; Matrosov, S.Y.; Schneider, T.L. Deriving mixed-phase cloud properties from Doppler radar spectra. *J. Atmos. Ocean. Technol.* **2004**, *21*, 660–670. [CrossRef]

27. Shupe, M.D.; Koliias, P.; Matrosov, M.; Eloranta, E. On deriving vertical air motions from cloud radar Doppler spectra. *J. Atmos. Ocean. Technol.* **2008**, *25*, 547–557. [CrossRef]

28. Liu, L.P.; Zheng, J.F.; Wu, J.Y. A Ka-band solid-state transmitter cloud radar and data merging algorithm for its measurements. *Adv. Atmos. Sci.* **2017**, *34*, 545–558. [CrossRef]

29. Zheng, J.F.; Liu, L.P.; Zeng, Z.M.; Xie, X.L.; Wu, J.Y.; Feng, K. Ka-band millimeter wave cloud radar data quality control. *J. Infrared Millim. Waves* **2016**, *35*, 748–757.

30. Hildebrand, P.H.; Sekhon, R.S. Objective determination of the noise level in Doppler spectra. *J. Appl. Meteorol.* **1974**, *13*, 808–811. [CrossRef]

31. Luke, E.P.; Kollias, P. Separating cloud and drizzle radar moments during precipitation onset using Doppler spectra. *J. Atmos. Ocean. Technol.* **2013**, *30*, 1656–1671. [CrossRef]

32. Petitdidier, M.; Sy, A.; Garrouste, A.; Delcourt, J. Statistical characteristics of the noise power spectral density in UHF and VHF wind profilers. *Radio Sci.* **1997**, *32*, 1229–1247. [CrossRef]

33. Bouniol, D.; Illingworth, A.J.; Hogan, R.J. Deriving turbulent kinetic energy dissipation rate within clouds using ground based 94 GHz radar. In Proceedings of the Preprints 31st International Conference on Radar Meteorology, Seattle, WA, USA, 7 August 2003; pp. 193–196.

34. O'Connor, E.J.; Hogan, R.J.; Illingworth, A.J. Retrieving stratocumulus drizzle parameters using Doppler radar and lidar. *J. Appl. Meteorol.* **2005**, *44*, 14–27. [CrossRef]

35. Warner, J. Time variation of updraft and water content in small cumulus clouds. *J. Atmos. Sci.* **1977**, *34*, 1306–1312. [CrossRef]

36. Gunn, R.; Kinzer, G.D. The terminal velocity of fall for water droplets in stagnant air. *J. Meteorol.* **1949**, *6*, 243–248. [CrossRef]

37. Foote, G.B.; Du Toit, P.S. Terminal velocity of raindrops aloft. *J. Appl. Meteorol.* **1969**, *8*, 249–253. [CrossRef]